Heat transfer intensification using an electrohydrodynamic plume on a MWCNT-thermal oil nanofluid

Rajab Al-Sayegh*

Departement of Mechanical Engineering, College of Engineering, Northern Border University, P.O. Box 1321, 91431, Arar, Saudi Arabia

* *Corresponding author; E-mail: rajab.alsayegh@nbu.edu.sa*

Abstract:

In this work the effect of an electrohydrodynamic plume in Rayleigh-Benard convection within an enclosure has been investigated. The enclosure is filled with a MWCNT-thermal oil nanofluid and subjected to a potential difference between a blade placed in the middle of the bottom wall and the top wall. The set of governing equations includes the Navier-Stokes, energy, charge density transport and Maxwell Gauss equations. The equations were solved using Patankar 's finite volume method. A detailed analysis dealing with the effect of the electrical Rayleigh number and the volume fraction of the nanoparticles was developed. It has been shown that the simultaneous use of two intensification techniques, namely the application of an electric field and the incorporation of a nanoparticles, can achieve an enhancement of the convective heat transfer by over 200%.

Key words*: numerical simulations, natural convection, heat transfer enhancement, nanofluid, electrohydrodynamic plume.*

1. INTRODUCTION

Heat transfer is a field that affects almost all industrial sectors: biology (Waqas et al. 2019), bio-medical (khan et al.2021), nanofluid (kolsi et al. 2021), biology and aerospace, ...

Concerning electrical - thermal coupling, the application of a potential difference between a blade electrode and a flat surface in a dielectric liquid allows the injection of electrical charges. These charges create an electric field which, in turn, creates an electric force called the coulomb force. When this force is high enough, it can break down the viscous forces and establish secondary electroconvective motions that can enhance heat transfer (Castellanos (1998)).

In recent years, this type of electrocovective jet has attracted a lot of attention not only for its numerous industrial applications such as heating, cooling and cleaning of electronic components, but also for its interesting geometry (very compact), its structure (simple) and its low energy consumption. Several experimental works have studied this EHD plume. Indeed, McCluskey and Perez (1992) were able to generate an electrohydrodynamic plume between a 3mm long blade and a stainless-steel plane placed at a distance of 10mm. The liquid used was silicone oil and the potential difference used was 20kV. The authors were able to record speeds of between 30 and 40 cm/s.

Yan et al. (2013) studied a planar blade actuator submerged in a dielectric liquid with a potential of 35kV and found that the coulomb force reached about 50±8mN/m in the longitudinal direction and 1.8±15mN/m in the transverse direction

Daaboul et al. (2009) investigate the injection of electrical charges into a blade-plane geometry. They applied negative and positive voltage echelons to observe the transient behaviour of the flow. The authors proved that a DC voltage produces a flow with a higher velocity than the AC voltage case. For AC voltages the low frequencies also generate a flow with moderate velocity while for high frequencies, no movement is generated.

Numerical work in the field of EHD plumes remains rather modest. Wu et al. (2013) present a numerical study for a 2D electrohydrodynamic flow between a hyperbolic blade and a flat electrode. A charge density non-autonomous injection law was considered and compared with the conventional autonomous injection law. The authors show the existence of a critical Reynolds number that separates the two flow regimes of stationary and unsteady flow.

Traore et al. (2014) undertook numerical research for the study of an EHD plume driven by a pointed blade electrode in a dielectric fluid. a parametric study taking into account different blade shapes, the electrical properties of the fluid and the injection level was established. Different flow regimes (stationary, transient and chaotic) have been recorded.

A two-dimensional numerical study was conducted by Wu et al. (2014) to estimate the heat transfer improvement due to EHD plumes in a cavity. It was found that the heat transfer efficiency can be considerably intensified by applying these EHD plumes. The local and mean Nusselt numbers are significantly enhanced up to 350%. Best performance can be achieved by raising the electrical Rayleigh number and the injection power setting.

One of the reasons that led us to study the electro-hydrodyconvection problem is that the generation of additional motion in the fluid. These instabilities due to electrical forces could be a promising way to intensify and control convective transfer. As a natural consequence, the use of this technique is increasing efficiency, reducing size and cost of the devices.

The phenomena of electrothermal convection (ETC) also occur in several important industrial processes (Wong et al. (2004)). New technologies in the field of microelectromechanics and nanotechnology are strongly related to ETC (De Voe et al. (2001); Gonzalez et al. (2003)).

Despite the considerable attention that has been given to the simulation of EHD plumes caused by the injection of unipolar charges (Vázquez et al. (2000)(2002)(2003)(2004),Perez et al. (2009), to our knowledge, none of them has dealt with the case of a dielectric nanofluid.

This work is a numerical contribution to the simulation of an electro-hydrodynamic plume in a dielectric nanofluid. All the coupled equations defining this problem is solved without simplifying assumptions by the volume method.

2. GOVERNING EQUATIONS AND NUMERICAL SOLUTION

We consider a square cavity of dimensions L2 (Figure 1) filled with an MWCNT-oil nanofluid. The cavity is exposed to a temperature difference between the hot bottom wall (T_H) and the cold top wall (T_C). In the middle of the bottom wall, a blade-type electrode is placed. An electric potential ($V = V_0 - V_1$) is then applied between the blade as the emitting electrode and the entire upper wall as the collecting electrode. The charge production is supposed as autonomous and homogeneous. In other words, the electric charge given by the emitter blade is assumed as constant and independent of time. The study is modelled by considering a Newtonian and incompressible nanofluid of density ρnf, kinematic viscosity νnf, electrical permittivity ε and ionic mobility K.

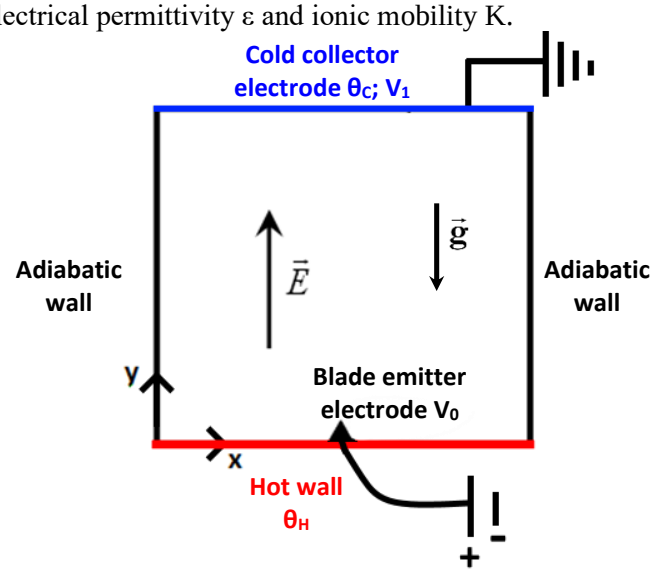

Figure 1. Physical model sketch

Based on the above assumptions up stated, the governing equations are (Hassen et al. (2020))

$$\nabla \vec{U} = 0 \tag{1}$$

$$\rho_{nf}\left(\frac{\partial \vec{U}}{\partial t} + \vec{U}.\nabla \vec{U}\right) = -\nabla p + \mu_{nf}\nabla^2 \vec{U} + \vec{g}\beta_{nf}\left(\theta - \theta_0\right) + q\vec{E} \tag{2}$$

$$\left(\rho C_p\right)_{nf}\left(\frac{\partial \theta}{\partial t} + \vec{U}.\nabla \theta\right) = \nabla \cdot \left(\lambda_{nf}\nabla \theta\right) \tag{3}$$

$$\frac{\partial q}{\partial t} + \nabla.\left[q\left(\vec{U} + K\vec{E}\right)\right] = 0 \tag{4}$$

$$\nabla \cdot \left(\varepsilon \vec{E}\right) = q \tag{5}$$

$$\vec{E} = -\nabla V \tag{6}$$

The vectors $\vec{U}$, $\vec{g}$ and $\vec{E}$ represent the fluid velocity field, the gravitational acceleration and the electric field, respectively. The scalars *p*, *q*, θ and *V* denote the pressure, electric charge density, temperature and electrical voltage, respectively.

The mathematical equations that define the thermophysical properties of MWCNT-oil are summarized below:

- Density (Kahveci (2010))

$$\rho_{nf} = \left(1-\varphi\right)\rho_f + \varphi\rho_s \tag{7}$$

- Viscosity [Pa.s] (Ilyas (2017))

$$\mu_{nf} = -1.8231 - \frac{0.0686}{T} + 1.7235\left(1-\varphi\right) + 3.329\left(1-\varphi\right)^2 + 136.7838\frac{\left(1-\varphi\right)^2}{T^2} - 3.2363\left(1-\varphi\right)^3 - 2347.39\frac{\left(1-\varphi\right)}{T^3} \tag{8}$$

- Thermal conductivity [$W.m^{-2}.K^{-1}$] (Ilyas (2017))

$$k_{nf} = 0.595 - 0.4547\left(1-\varphi\right) + T\left(0.7422 - 0.606\left(1-\varphi\right) + \frac{0.2759}{\left(1-\varphi\right)} - \frac{0.3943}{\left(1-\varphi\right)^2}\right) \tag{9}$$

- Specific heat [$kJ.kg^{-1}.K^{-1}$] (Ilyas (2017))

$$Cp_{nf} = -20 + 21.573\left(1-\varphi\right) - 0.012T + 0.024\left(1-\varphi\right) \tag{10}$$

- Thermal expansion coefficient [K^{-1}] (Ilyas (2017))

$$\beta_{nf} = 7.56.10^{-4} + 6.34\times10^{-7}T - 8.09.10^{-4}\varphi \tag{11}$$

Thermophysical properties of the thermal oil and nanoparticles are illustrated in Table1.

Table 1. Thermophysical characteristics of base fluid and nanoparticles (Ilyas (2017))

	Thermal oil	MWCNT
ρ [kg/m^3]	854.5	2100
C_p [J/(kg.K)]	1970	733
λ [W/(m.K)]	0.133	2000

Using "stream function–vorticity" (ψ-ω) formulation and introducing the following dimensionless variables:

$$x^* = \frac{x}{L} \qquad y^* = \frac{y}{L} \qquad U_1^* = U_1 \frac{L}{\alpha_f} \qquad U_2^* = U_2 \frac{L}{\alpha_f} \qquad \psi^* = \frac{\psi}{\alpha_f} \qquad \omega^* = \omega \frac{L^2}{\alpha_f}$$

$$t^* = t \frac{\alpha_f}{L^2} \qquad \theta^* = \frac{\left(\theta - \theta_f\right)}{\left(\theta_H - \theta_C\right)} \qquad q^* = \frac{q}{q_0} \qquad E^* = E \frac{L}{\left(V_0 - V_1\right)} \qquad V^* = \frac{\left(V - V_1\right)}{\left(V_0 - V_1\right)}$$

The equation system (1)–(5) becomes (the star marker is removed for better simplicity) (Hassen et al. (2020)):

$$\omega = -\left(\frac{\partial^2 \Psi}{\partial x^2} + \frac{\partial^2 \Psi}{\partial y^2} \right) \tag{12}$$

$$\frac{\partial \omega}{\partial t} + U_1 \frac{\partial \omega}{\partial x} + U_2 \frac{\partial \omega}{\partial y} = \frac{\mu_{nf} / \mu_f}{\rho_{nf} / \rho_f} Pr \left(\frac{\partial^2 \omega}{\partial x^2} + \frac{\partial^2 \omega}{\partial y^2} \right) + \frac{\beta_{nf}}{\beta_f} Ra \cdot Pr \frac{\partial \theta}{\partial x} + \frac{\rho_{nf}}{\rho_f} \frac{CT^2}{M^2} \cdot Pr^2 \left(\frac{\partial \left(qE_1\right)}{\partial x} + \frac{\partial \left(qE_2\right)}{\partial y} \right) \tag{13}$$

$$\frac{\partial \theta}{\partial t} + U_1 \frac{\partial \theta}{\partial x} + U_2 \frac{\partial \theta}{\partial y} = \frac{\alpha_{nf}}{\alpha_f} \left(\frac{\partial^2 \theta}{\partial x^2} + \frac{\partial^2 \theta}{\partial y^2} \right) \tag{14}$$

$$\frac{\partial q}{\partial t} + \frac{\partial q}{\partial x} \left(q \left(U_1 + \frac{T \cdot Pr}{M^2} \cdot E_1 \right) \right) + \frac{\partial q}{\partial y} \left(q \left(U_2 + \frac{T \cdot Pr}{M^2} \cdot E_2 \right) \right) = 0 \tag{15}$$

$$\frac{\partial^2 V}{\partial x^2} + \frac{\partial^2 V}{\partial y^2} = -C \cdot q \tag{16}$$

$$E_1 = -\frac{\partial V}{\partial x} \quad E_2 = -\frac{\partial V}{\partial y} \tag{17)(18}$$

The dimensionless study of the above equations involves five dimensionless numbers defined as follows:

$$Ra = \frac{g \beta_f \Delta \theta L^3}{\alpha_f \nu_f} \quad Pr = \frac{\nu_f}{\alpha_f} \qquad T = \frac{\varepsilon \Delta V}{\rho_f \nu_f K} \qquad C = \frac{qL^2}{\varepsilon \Delta V} \qquad M = \frac{1}{K} \left(\frac{\varepsilon}{\rho_f} \right)^{1/2}$$

The thermal Rayleigh number (Ra) is the quotient of thermal force to friction force; the electrical Rayleigh number (T) is the quotient of electrical force to friction force; Prandtl number (Pr) is the ratio of friction to heat diffusivity; C is the injection level, and the mobility number (M) which defines the electrical properties of the fluid.

The dimensionless boundary conditions are:

- Vertical adiabatic walls (x=0) and (x=1)

$$\Psi = \frac{\partial \Psi}{\partial x} = 0 \qquad \frac{\partial \theta}{\partial x} = 0 \qquad \frac{\partial q}{\partial x} = 0 \qquad \frac{\partial V}{\partial x} = 0$$

- Bottom hot wall (excluding blade) (y=0)

$$\Psi = \frac{\partial \Psi}{\partial y} = 0 \qquad \theta = 1 \qquad \frac{\partial q}{\partial y} = 0 \qquad \frac{\partial V}{\partial y} = 0$$

- Top cold wall (collector electrode) (y=1)

$$\Psi = \frac{\partial \Psi}{\partial y} = 0 \qquad \theta = 0 \qquad \frac{\partial q}{\partial y} = 0 \qquad \frac{\partial V}{\partial y} = 0$$

- Blade (Emitter electrode) (x=0.5; y=0)

$$\Psi = \frac{\partial \Psi}{\partial y} = 0 \qquad \theta = 1 \qquad q = 1 \qquad V = 1$$

The local Nusselt number is calculated as follows:

$$Nu_{loc} = -\left(\frac{\lambda_{nf}}{\lambda_f}\right)\left.\frac{\partial \theta}{\partial y}\right|_{y=0} \tag{19}$$

The mean Nusselt number on the bottom wall, is expressed by

$$Nu_m = \int_0^1 -\left(\frac{\lambda_{nf}}{\lambda_f}\right)\left.\frac{\partial \theta}{\partial y}\right|_{y=0} dx \tag{20}$$

The system of equations (12) and (18) under the associated boundary conditions is numerically using an in-house code developed on Fortran 90. The finite volume method of Patankar (1980) has been adopted. After discretization, the iterative method applied for the resolution of the algebraic system equations is the Gauss-Seidel method, with a sub-relaxation process. The mesh size adopted is 101x101, the time step and the convergence criteria have been set at 10^{-4} and 10^{-6}.

The following test is used to check the convergence:

$$\frac{max\left|\psi^n - \psi^{n+1}\right|}{max\left|\psi^n\right|} + max\left|\theta^n - \theta^{n+1}\right| + max\left|q^n - q^{n+1}\right| \le 10^{-5} \tag{21}$$

Additional numerical details are available in Hassen et al. (2013).

3. VALIDATION TEST

To validate our code we studied the configuration of Wu et al. (2014). It consists of a two-dimensional cavity partially heated by the top wall and equipped with a blade centred on the cold bottom wall. This blade generates an electric charge injection generated by a potential difference applied between this blade and the top wall.

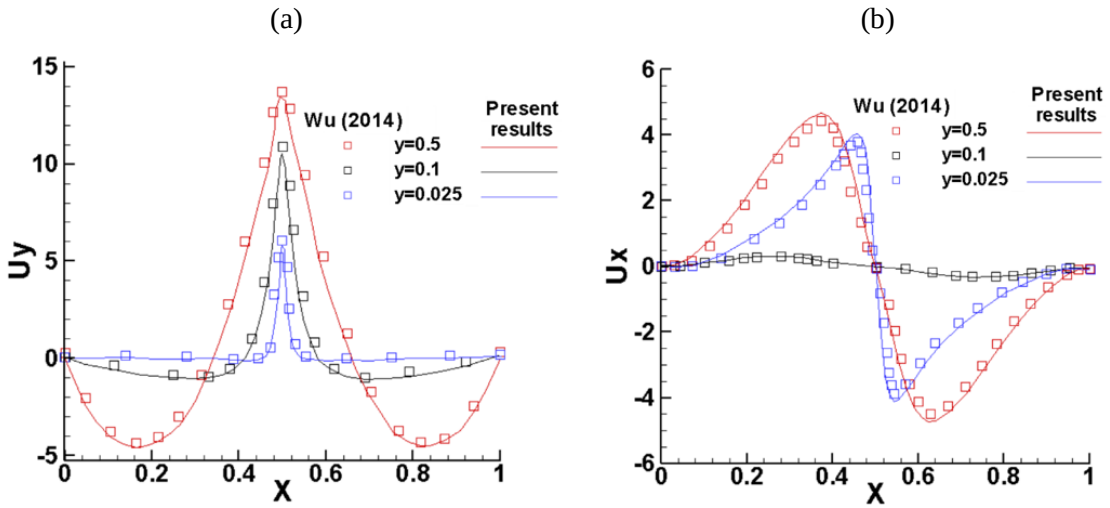

Figure 2. velocity profile for C = 10 and T = 1000. (a) Horizontal velocity; (b) Longitudinal velocity.

4. RESULTS AND DISCUSSION

In this numerical study, we focus on the effect of an electrohydrodynamic plume on Rayleigh-Benard convection in a closed enclosure. The main parameters are the electrical Rayleigh number and the volume fraction of the nanoparticles. The results presented include the electric charge density, the current function, the temperature distributions and the variation of the Nusselt number.

As expected, the charge density distribution (Figure 3) reveals that the greatest accumulation of electric charge remains around the injector blade, and it can also be seen that the electrical forces generated by the potential differences between the blade and the plane drive the electrical charges towards the upper receiving electrode. This migration causes the formation of a so-called electrohydrodynamic plume and create an electro-convective current similar to an axisymmetric jet. It should be noted that the greater the electrical Rayleigh number, the greater the injection, penetration, and the velocity of the electrical charges. Indeed, as shown in figure 4 (a) the charge penetration is more important while the width of the plume decreases with T. This could be explained by the fact that the inertial forces moving upwards dominate the diffusion forces, which minimizes the lateral charge dispersion. Figure 4 (b) which illustrates the distribution of the electric charge density at the centre of the plume supports the fact that the charge concentration inside the cavity increases with the electric Rayleigh number. Actually, on the collecting electrode (upper wall) y=1 the charge density goes from 0.15 at T=50 to 0.27 at T=300, i.e. an increase of 80%.

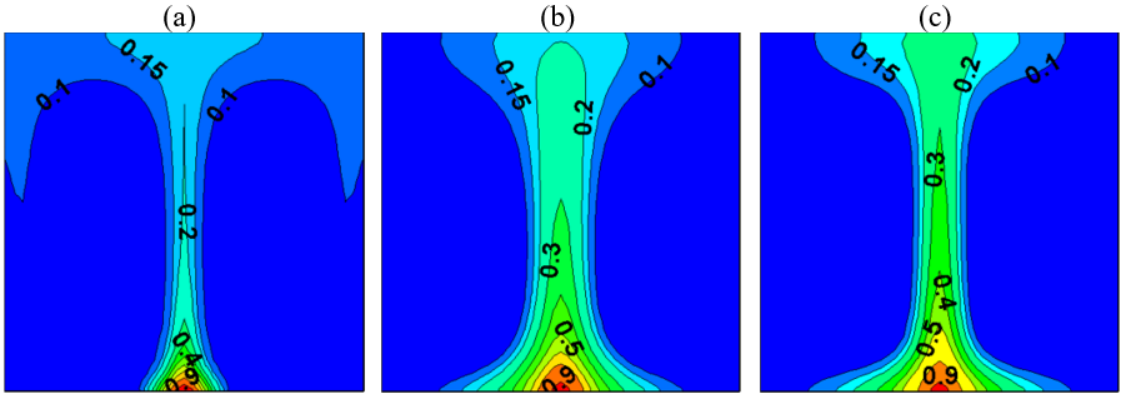

Figure 3. Electric charge density distribution for Ra = 10^4 and φ = 0.5% for different values of the electric Rayleigh number: T=50 (a), 200 (b), 400 (c)

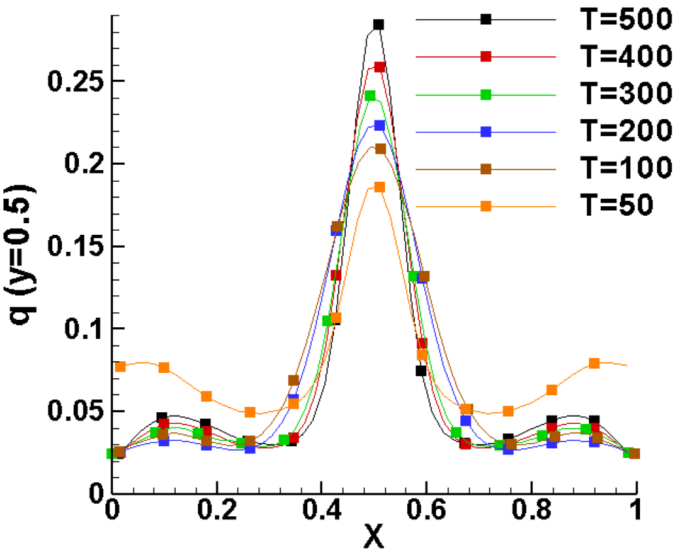

(a)

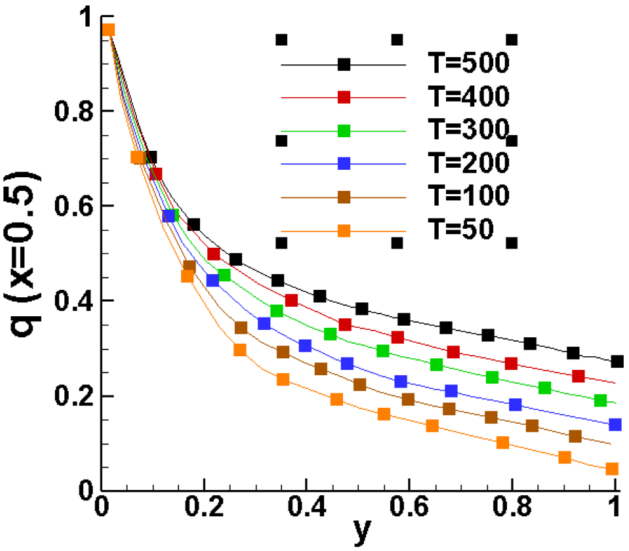

(b)

Figure 4. Charge density profile at the centre of the enclosure (Ra=10^4 and φ=0.5%)
(a): y= 0.5 (b): x= 0.5

The distribution of the streamlines (Figure 5) indicates the presence of a bicellular flow marked by two symmetrical and counter-rotating cells. During their displacement from the blade to the upper plate, the electric charges plume carries the nanofluid with it and therefore creates a movement (even a jet) quite important. Hence, on both sides of this plume there is a generation of the two observed counter-rotating cells. The rotational vortex velocity is strongly affected by the electrical Rayleigh number. By increasing T from 50 to 400 the vortex intensity is enhanced by a factor of six. All these results are approved by figure 6 which displays the vertical velocity profile at the centre of the cavity for different values of electrical Rayleigh and at different positions from the blade. By examining this figure, it can be seen that the velocity pattern is similar to a free jet with a peak in the centre and recirculation zones on the sides. These results were also observed experimentally in the work of McCluskey et al. (1992).

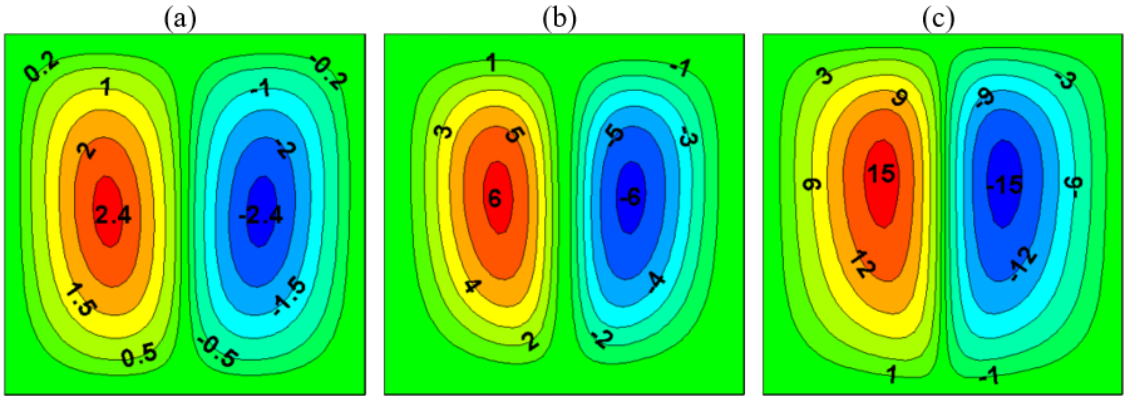

Figure 5. Streamlines distribution for Ra=10^4 and φ=0.5% and for different values of the electric Rayleigh number: T=50 (a), 200 (b), 400 (c)

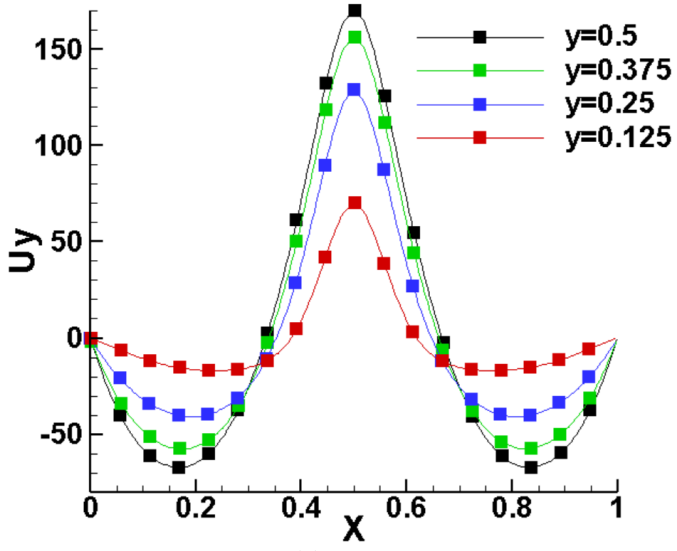

(a)

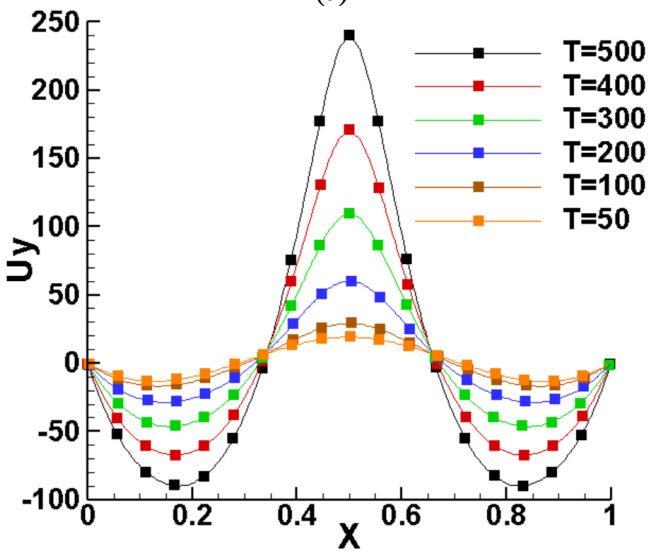

(b)

Figure 6. Vertical velocity profile for Ra=10^4 and φ=0.5%
(a): for different distances from the blade; (b): for different electric Rayleigh values

The isotherms illustrated in Figure 7 show the formation of a thermal mushroom, which produces a strong upward penetration of the hot layers in the centre of the cavity with a return of the cold fluid layers near the vertical walls. It can also, be seen that the distribution of isotherms is also strongly influenced by the strength of the electrical forces. By increasing T almost, the entire cavity is submerged by the hot fluid and the distortion of the isothermal lines becomes more pronounced.

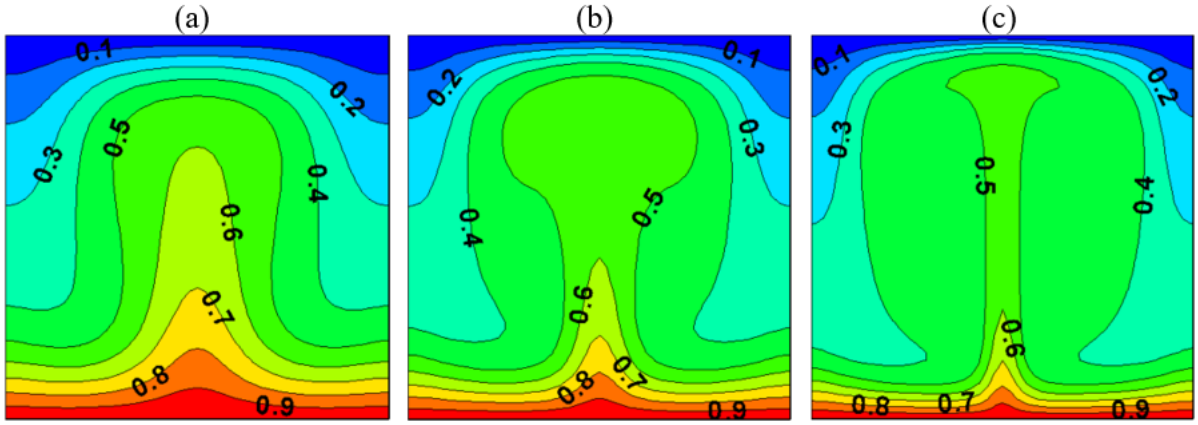

Figure 7. Isotherm distribution for Ra=10^4 and φ=0.5% for different values of the electric Rayleigh number: T=50 (a), 200 (b), 400 (c)

Figure 8 records the variation of convective heat transfer as a function of the nanoparticle volume fraction and electrical Rayleigh number. A transfer improvement of between 68% and 160% can be reached by varying the electric Rayleigh number from 20 to 600 and an enhancement of 15% up to 80% is recorded by varying the fi from 0 to 0.5%. Finally, a double intensification of more than 200% can be achieved by the simultaneous addition of nanoparticles and an electric field.

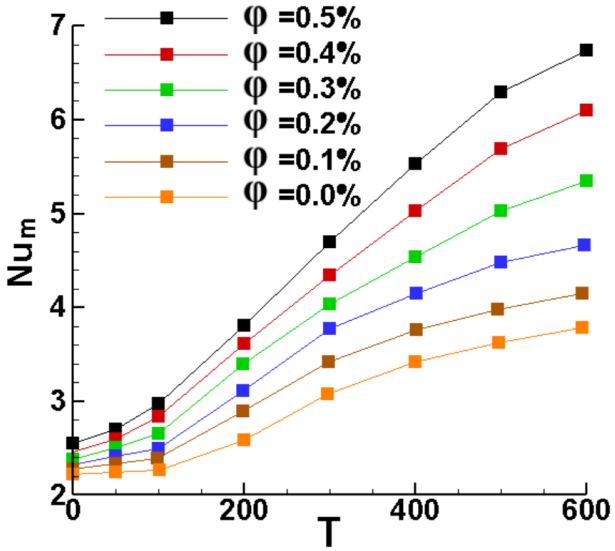

Figure 8. Average Nusselt number profile T for Ra=10^4 and various values of nanoparticle volume fractions.

CONCLUSION

This work focuses on the study of heat transfer intensification using an electrohydrodynamic plume on a MWCNT -Dielectric nanofluid. The Rayleigh-Benard configuration with a blade placed in the middle of the hot wall was treated. The equations were solved using Patankar's finite volume method with a mesh size of 101x101.
Main findings were drawn as below:

- Depending on the applied electric potential between the blade and the collector plane a significant charge injection takes place.
- The injection of electrical charges generates an electro-hydrodynamic flow that creates a strong pumping action and a movement similar to that of a free jet.
- A multi-cell flow made up of two counter-rotating vortex is then established on either side of the electro-hydrodynamic plume.
- The plume allows the penetration of hot fluid layers with a mushroom shape inside the cavity.
- The addition of MCWNT nanoparticles improves convective heat transfer by up to 80%.
- The electric field can increase the convective heat transfer by up to 160%.
- The simultaneous use of nanoparticles and electric fields allows reaching an intensification of over 200%.

As a future outlook, this work can be expanded by taking into account the following recommendations

- The position of the blades giving the best heat transfer should be optimised.
- The case of charge injection by several blades needs to be explored.
- The effect of other types of pure and hybrid nanofluids can be examined.

References

Castellanos, A., 1998.electrohydrodynamics. Springer-Verlag,.(ISBN 3-211-83137-1)

Daaboul, M., Louste, C., Romat, H., 2009. Transient velocity induced by electric injection in blade-plane geometry, Journal of Electrostatics 67, p. 359.

De Voe, D. L., Darabi, J., Ohadi, M., 2001. An electrohydrodynamic polarization micropump for electronic cooling applications, J. Microelectromech. Syst. 10, p. 98.

Gonzalez, A., Green, N. G., Castellanos, A., Ramos, A., Morgan, H., 2003. Electrohydrodynamics and dielectrophoresis in microsystems: scaling laws, J.Phys. D: Appl. Phys. 36, p. 2584.

Hassen, W., Borjini, M.N., Traore, P., Aissia, H. B., 2013. Electroconvection between Coaxial ylinders of Arbitrary Ratio Subjected to Strong Unipolar Injection, Journal of Electrostatics 71, p. 882.

Hassen, W., Kolsi, L., Mohammed, H. A., Ghachem, K., Sheikholeslami, M., Almeshaal, M. A., 2020. Transient electrohydrodynamic convective flow and heat transfer of MWCNT-Dielectric nanofluid in a heated enclosure, Physics Letters A 384, p. 126736.

Ilyas, S.U., Pendyala, R., Narahari, M., 2017. Stability and thermal analysis of MWCNT-thermal oil-based nanofluids, Colloid Surface A. 527, p. 11.

Kahveci, K., 2010. Buoyancy driven heat transfer of nanouids in a tilted enclosure, Journal of Heat Transfer 132, p.1.

Khan, S. U., Al-Khaled, K., Bhatti, M. M., 2021. Numerical experiment of Reiner–Philippoff nanofluid flow subject to the higher-order slip features, activation energy, and bioconvection. Partial Differ. Equations Appl. Math. 4, p. 100126.

Kolsi, L., Abbasi, A., Alqsair, U. F., Farooq, W., Omri, M., Khan, S. U., 2021. Thermal enhancement of ethylene glycol base material with hybrid nanofluid for oblique stagnation point slip flow, Case Stud. Therm. Eng. 28, p. 101468.

Kolsi, L., Dero, S., Lund, L. A., Alqsair, U. F., Omri, M., Khan, S. U., 2021. Thermal stability and performances of hybrid nanoparticles for convective heat transfer phenomenon with multiple solutions, Case Stud. Therm. Eng. 28, p. 101684.

McCluskey, F.M.J, Perez, A.T., 1992. The electrohydrodynamic plume between a line source of ions and a flat plate, IEEE Transactions on electrical insulation 27, p.334.

Patankar, S.V., 1980. Numerical Heat Transfer and Fluid Flow, McGraw-Hill, Washing-ton, DC.

Pérez, A. T., Traoré, P., Koulova-Nenova, D., Romat, H., 2009. Numerical study of an electrohydrodynamic plume between a blade injector and a flat plate, IEEE Transactions on Dielectrics and Electrical Insulation 16, p. 448.

Traore, P., Wu, J., Louste, C., Pelletier, Q., Dascalescu, L., 2014. Electrohydrodynamic plumes due to autonomous and nonautonomous charge injection by a sharp blade electrode in a dielectric liquid. IEEE Transactions on Industry Applications 51, p. 2504.

Vázquez, P. A, Castellanos, A., Pérez, A. T., Chicon R., 2000. Numerical modelling of EHD flows due to injectors of finite size, in Proc. Conf. Elect. Insul. Dielectr. Phenom. 1, p. 101.

Vázquez, P. A., Vera, E. C., Castellanos A., Rebollo, T. C., 2002. Finite element-particle method calculation of EHD plumes, in Proc. Annu. Rep. Conf. Elect. Insul. Dielectr. Phenom., Cancun, Mexico, p. 208.

Vázquez, P. A., Vera, E. C., Castellanos, A., Rebollo, T. C., 2003 Numerical calculations of two-dimensional EHD plumes with finite element and particle methods, in Proc. Annu. Rep. Conf. Elect. Insul. Dielectr. Phenom., Albuquerque, NM, USA., p. 706.

Vázquez, P. A., Soria C., and Castellanos A., 2004. Numerical simulation of two-dimensional EHD plumes mixing finite element and particle methods, in Proc. Annu. Rep. Conf. Elect. Insul. Dielectr. Phenom., p. 122.

Waqas, H., Khan, S. U., Hassan, M., Bhatti, M. M., Imran, M., 2019. Analysis on the bioconvection flow of modified second-grade nanofluid containing gyrotactic microorganisms and nanoparticles, J. Mol. Liq. 291, p. 111231.

Wong, P. K., Wang, T.H., Deval, J. H., Ho, C. M., 2004. Electrokinetics in micro devices for biotechnology applications. IEEE/ASME Trans. Mechatro., P.9366.

Wu, J., Traore, P., Louste, C., Koulova, D., Romat, H., 2013. Direct numerical simulation of electrohydrodynamic plumes generated by a hyperbolic blade electrode, Journal of Electrostatics 71, p. 326.

Wu, J., Traoré, P., Louste, C., Dascalescu, L., Tian, F. B., Pérez, A. T., 2014. Numerical investigation of electrohydrodynamic plumes for locally enhanced cooling in dielectric liquids. IEEE Transactions on Industry Applications 51, p.669.

Yan, Z., Louste, C., Traoré, P., Romat, H., 2013. Experimental estimation of the electric force induced by a blade-plane actuator in dielectric liquids, Journal of Electrostatics 71 p. 478.